ELSEVIER

Journal of Power Sources 63 (1996) 33–39

JOURNAL OF POWER SOURCES

Electroreduction of graphite in $LiClO_4$–ethylene carbonate electrolyte. Characterization of the passivating layer by transmission electron microscopy and Fourier-transform infrared spectroscopy

A. Naji [a], J. Ghanbaja [a], B. Humbert [b], P. Willmann [c], D. Billaud [a]

[a] *Laboratoire de Chimie du Solide Minéral, Université Henri Poincaré, Nancy I, BP 239, 54506 Vandoeuvre-lès-Nancy Cedex, France*

[b] *CNRS-UHP, LCPE, 54600 Villers-lès-Nancy, France*

[c] *CNES, 18 avenue E. Belin, 31055 Toulouse Cedex, France*

Received 1 February 1996; revised 18 May 1996; accepted 10 June 1996

Abstract

Electrochemical intercalation of unsolvated lithium into pitch carbon fibres P100 and natural graphite UF_4 has been carried out in $LiClO_4$–ethylene carbonate electrolyte. The reversible electrochemical capacity for a current equal to 7 μA/mg is 260 mAh/g for P100 carbon fibres and about 350 mAh/g for UF_4 graphite, respectively. During the first discharge (reduction) an electrochemical capacity greater than the theoretical value (372 mAh/g) corresponding to LiC_6 is obtained. This excess of capacity can be related to the formation of a passivating layer on the carbon surface. Analysis of this layer by means of transmission electron microscopy (electron diffraction, electron energy loss spectroscopy, and imaging) and Fourier-transform infrared spectroscopy has shown that this layer is composed of lithium carbonate Li_2CO_3 and alkylcarbonates of lithium $ROCO_2Li$. Formation of Li_2CO_3 occurs at potentials in the 1–0.8 V range versus Li^+/Li, and formation of lithium alkylcarbonates then follows at potentials below 0.8 V. We then attributed the voltage plateau at 0.9 V versus Li^+/Li observed in the electrochemical waves to the reduction of ethylene carbonate into Li_2CO_3. Transmission electron spectroscopy revealed the presence of lithium chloride in the electrolyte which appears as small rods.

Keywords: Electroreduction; Graphite; Pitch fibres; Ethylene carbonate

1. Introduction

During the past years, tremendous efforts have been dedicated to the development of secondary 'lithium-ion' batteries. In this technology a positive electrode made of transition metal oxides (Li_xNiO_2, $Li_xMn_2O_4$, Li_xCoO_2, $Li_xV_2O_5$) is associated with a carbon anode in an organic electrolyte [1,2]. The use of intercalation compounds of lithium into carbon [3] allows to overcome the limitations of reversibility observed with electrodes made from lithium metal [4].

By associating these intercalation compounds with highly oxidizing lamellar oxides one may obtain batteries with energy densities up to three times higher than those of Ni/Cd cells and being able to achieve more than 1000 charge/discharge cycles [2].

The stoichiometry of these lithium intercalation compounds is strongly dependent on the nature of the carbon used [5,6] and the composition of the electrolyte [3,7].

When propylene carbonate (PC) based electrolytes are used, direct intercalation of lithium into graphite will not occur [8]. In this case, the degradation of the graphite electrode is supposed to be a consequence of (i) its exfoliation related to the decomposition of PC (CH_3–CH=CH_2 gaseous evolution between the graphene sheets) and (ii) a likely electrical insulation of the isolated exfoliated parts of the electrode [8–10].

In the case of ethylene carbonate (EC) based electrolytes, no exfoliation occurs and unsolvated lithium intercalation is observed leading to formation of the LiC_6 compound similar to that prepared by a direct reaction of metallic lithium onto graphite [11,12]. Previous studies [3,13–15] have shown that during the first discharge a part of the reduction current is consumed by the electrolytic reduction at the surface of carbon with formation of a passivating layer. The nature of this layer has been studied by means of Fourier-transform infrared spectroscopy (FT-IR) and it is shown that the use of additives may modify significantly its properties and in some cases (CO_2) improve the performances of the carbon electrode [14,16].

In this study we investigated the electrochemical properties of two types of carbon which appear to be suitable for prac-

0378-7753/96/$15.00 © 1996 Elsevier Science S.A. All rights reserved
PII S0378-7753(96)02439-1

tical applications. The passivating surface layer has been studied by associating transmission electron microscopy (TEM) and FT-IR analysis.

2. Experimental

Two types of carbon materials were used: Pitch carbon fibres P100 (Amoco) and natural graphite UF_4 (Le Carbone Lorraine). Their characteristics (specific BET area, coherence lengths L_c along c-axis and interplanar spacing d_{002}) are given in Table 1. Samples of P100 fibres are outgassed under vacuum at 700 °C and thoses of UF_4 graphite at 430 °C. In order to remove their protective film higher temperatures were used for P100 fibres. Lithium perchlorate $LiClO_4$ (Aldrich, purity 95%) and EC (Fluka, purity > 99%) powder were outgassed under dynamic vacuum at 150 and 20 °C, respectively. Intercalation was performed in a two-electrode cell with lithium foil acting simultaneously as the counter and the reference electrodes. The working electrode is made of either milled P100 fibres or UF_4 graphite powder both being mixed with polyvinylidene difluoride (PVDF) as the binder (10% w/w or 3% w/w for infrared (IR) and TEM studies). The electrolyte used was a solution of $LiClO_4$ in EC (1.5 M EC) in which the water content was lower than 50 ppm. A multi-channel microprocessor-controlled Mac Pile potentiostat/galvanostat was used for the electrochemical experiments. The potentials referred to an Li^+/Li electrode. X-ray diffraction (XRD) studies were carried out using a rotating anode (RIGAKU RU-200 B, Mo Kα radiation) coupled with a curved detector (INEL CPS 120). The coherence lengths L_c were calculated from the half-height width of the (004) reflections, using the Scherrer's relation. The BET areas were measured on a Micrometric ASAP 2300 equipment using a mixture of 70% of helium and 30% of nitrogen as the analysis gas.

TEM studies electron energy loss spectroscopy (EELS) and small angle electron diffraction (SAED) were conducted on a CM 20 Philips microscope equipped with a parallel EEL spectrometer (Gatan 666). Samples previously ground were deposited on copper grids covered with a holey amorphous carbon layer. A low temperature sample holder was used in order to limit the effects of heating of the electron beam on the samples.

The atomic concentration ratio O/C of oxygen and carbon is determined by the following equation [17,18]

$$O/C = I_O \sigma_C(\alpha,\Delta E)/I_C \sigma_O(\alpha,\Delta E) \quad (1)$$

Table 1
Characteristics of the two types of carbon materials used

Carbon	L_c (nm)	Surface area (m^2/g)	d_{002} (nm)
P100	9	76	0.338
UF_4	> 100	10	0.335

where O and C are the number of atoms of oxygen and carbon per unit area, respectively; I_O (α, ΔE) and I_C (α, ΔE) are the core loss intensities integrated up to an energy of width ΔE starting at the edge onset, σ_O (α, ΔE) and σ_C (α, ΔE) are the partial ionization cross sections integrated over the acceptance angle α and ΔE is an energy region.

A typical value for ΔE in the energy region lies within 50–100 eV. The accuracy of atomic concentration ratio is lower than 10%.

FT-IR studies were performed with a Fourier-transform spectrometer (Perkin-Elmer 2000). The following techniques were used to record the sample spectra:

(i) Diffuse reflection with a Harrick HVC accessory allowing to obtain spectra of samples mixed with KCl (3% w/w) under evacuated atmosphere (10^{-2} mbar) and at various temperatures between 20 and 60 °C. Recording spectra under vacuum needs the use of an IR CaF_2 window which, in turn, reduces the intensity of the signal for frequencies lower than 900 cm^{-1}. The sample spectra obtained by this technique are presented in this work as the result of the substraction of the original spectrum and that of a KCl reference. The absorbance is plotted as log (R_r/R_s) where R_s is the monobeam reflectance of the sample and R_r is the diffuse reflectance of KCl. It should be noticed that the diffuse reflection method is not really quantitative but it allows to follow the evolution of the reflection.

(ii) Transmission in dry air atmosphere through a pastille made of a few milligrams of sample materials mixed with KBr. In this case, the quantitative Lambert–Beer law is applicable in a first approach.

3. Results and discussion

3.1. Electrochemical studies

Fig. 1 shows the five first charge/discharge cycles under galvanostatic conditions (7 μA/mg) for an electrode made of ground P100 fibres and PVDF (10% w/w). The initial open-circuit potential of the sample, placed in the electrolyte, is about 3 V versus Li^+/Li. For the first discharge (Fig. 1(a)), the only voltage plateau which appears at about 0.9 V is attributed to the reduction of the electrolyte with formation of a passivating layer [3,19]. The discharged capacity recorded at this first cycle exceeds largely the theoretical value corresponding to LiC_6. This excess of current consumed is due to the formation of the passivating layer and also, in our case, to a possible reduction of the PVDF binder. A slight irreversible capacity is observed in the second cycle. For the third cycle, the reversible capacity corresponds to 70% (260 mAh/g) of the theoretical value as shown in Fig. 1(b).

Fig. 2 displays the four first cycles obtained with a UF_4–PVDF electrode in the same sample conditions as in Fig. 1. A strong diminution of the discharged capacity between the first and the second cycles is observed for the P100 fibres.

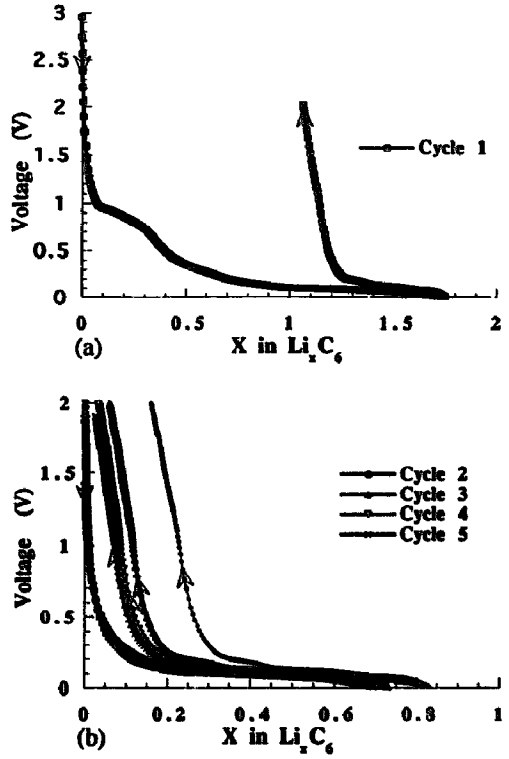

Fig. 1. Charge and discharge curves of the composite electrode P100–PVDF (10% w/w) in EC–$LiClO_4$ (1.5 M EC) with a specific current equal to 7 μA/mg, T=20 °C.

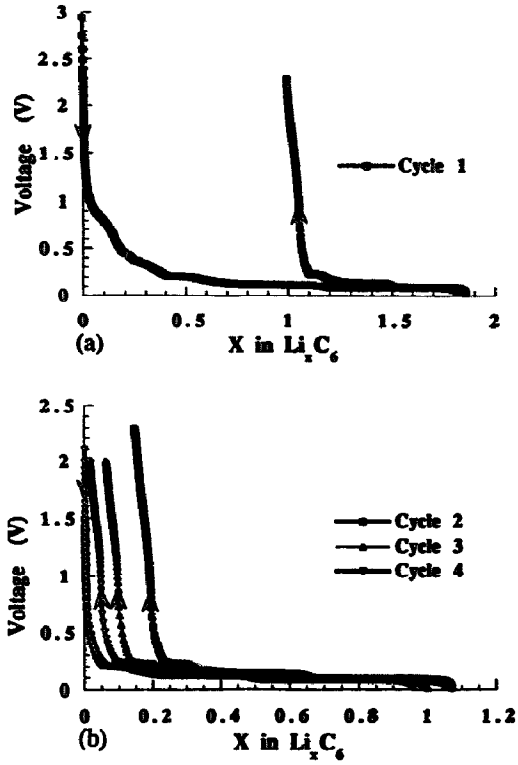

Fig. 2. Charge and discharge curves of the composite electrode UF_4–PVDF (10% w/w) in EC–$LiClO_4$ (1.5 M EC) with a specific current equal to 7 μA/mg, T=20 °C.

For the first cycle (Fig. 2(a)), the discharged capacity is greater than the theoretical value of LiC_6, but the values recorded for the next cycles (between 2 and 0.01 V) are close to this value (350 mAh/g), see Fig. 2(b).

In the case of the UF_4–PVDF electrode, the electrochemical curves exhibit several plateaus corresponding to the formation of lithium graphite intercalation compounds of various stages [3,11]. For the P100 fibre electrode, voltage plateaus are less noticeable and appear mainly in the oxidation process. The voltage and the reversible capacity differ when graphite or carbon fibres are used as the host. The different behaviours between these carbonaceous materials are related to their structural organization. In particular, the structure of carbon fibres includes the turbostratic disorder which influences the electrochemical performance [3]. Yazami et al. [20] who used several carbon fibres of different origins found that the reversible capacity increases with their crystallinity. In both cases, a great part of the discharged current during the first reduction is used for the formation of the passivating layer. The irreversible capacity (difference between the capacity in the reduction process and that in the oxidation one) of the P100–PVDF and UF_4–PVDF electrodes between 2 and 0.01 V is equal to 396 and 367 mAh/g, respectively. It should be noticed that the partial irreversible capacity calculated along the pseudo-potential plateau at 0.9 V (between 1 and 0.75 V) is 81 mAh/g. Similar behaviour are obtained for the UF_4 electrode. It is then obvious that the formation of the passivating layer is not completely achieved at the end of the pseudo-plateau but continues at lower potentials. This suggests that the formation of the passivating layer occurs at least in two steps.

Then, we studied the surface layer obtained at a potential of 0.8 V (first plateau) and for lower potential values around 0.01 V (intercalation domain).

3.2. TEM studies

TEM observations of the graphite used, after a complete first charge/discharge cycle (between 2 and 0.01 V), show that the carbon surface is covered with a thin spongy layer. For example, Fig. 3 shows the TEM micrograph of the UF_4 electrode before (Fig. 3(a)) and after a first charge/dicharge cycle (Fig. 3(b)) in EC–$LiClO_4$. This passivating layer allows the lithium ions to intercalate into graphite but blocks therefore the solvent molecules avoiding their co-intercalation [3,16,21].

Fig. 4 gives the ED diagram of graphite covered by the passivating layer shown in Fig. 3. Diffraction spots observed are characteristic of the hexagonal structure of unintercalated graphite. Diffraction rings correspond to a poly-crystalline phase and their indexation is in agreement with the monoclinic structure of Li_2CO_3.

The diffraction patterns obtained do not allow to identify other phases such as lithium alkylcarbonates. This may be

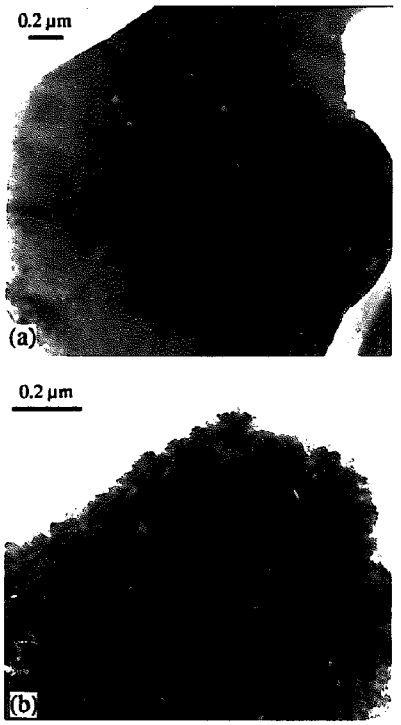

Fig. 3. TEM micrograph of the UF_4 electrode (a) before and (b) after a first charge/discharge cycle in EC–$LiClO_4$ (1.5 M EC), $T = 20$ °C.

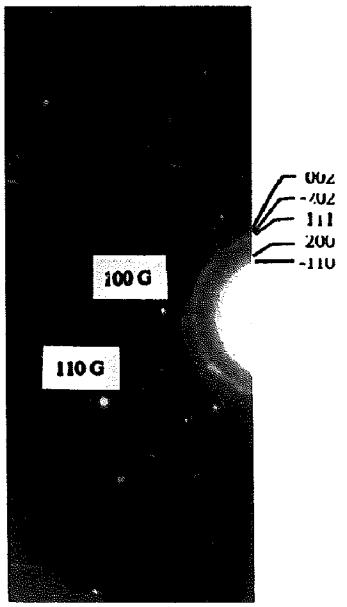

Fig. 4. Electron diffraction pattern of graphite covered by the passivating layer presented in Fig. 3(b).

due to the fact that these alkylcarbonates are either in an amorphous state or that they are produced in too little quantities suitable to observe diffraction.

In order to characterize these phases, EELS has been performed on an UF_4–PVDF electrode (97–3% w/w) reduced to 0.01 V and then oxidized up to 2 V. In all cases, analysis was done on different particles of the passivating layer placed above the holes of the grid in order to avoid parasitic signals due to the amorphous carbon of the grid and to the graphite of the electrode.

Fig. 5 (a)–(c) presents the energy loss spectra at the K-edge of carbon for three different selected parts of the passivating layer. Each spectrum exhibits two peaks at 289 and 299 eV related to the electronic transitions of the (1s) atomic carbon orbitals towards the vacant antibonding molecular π^* and σ^* orbitals corresponding respectively to the C=O and C–O bonds.

This fine structure at the K-edge level (ELNES) is characteristic for that of a carbonate as supported by the EEL spectrum of Li_2CO_3 presented in Fig. 6(a). The atomic O/C ratio determined for the three spectra in Fig. 5(a)–(c) are 2.8, 1.5 and 1, respectively.

The EEL spectrum in Fig. 5(d) is typical for the Li^+ cation, with an ionization edge of about 60 eV. Such a spectrum is comparable with that of Li_2CO_3 at the lithium K-edge shown in Fig. 6(b).

Therefore, the spectrum shown in Fig. 5(a) which is very similar to that of Li_2CO_3 can be attributed to this phase. This conclusion is supported by the presence of the diffraction rings present in the ED diagram in Fig. 4 and is typical of Li_2CO_3.

The spectra in Fig. 5(b) and (c) can be attributed to the lithium alkylcarbonates ($ROCO_2Li$). In these spectra, the peak at 299 eV is larger and more intense than that presented in Fig. 5(a). This is probably related to a modification of the chemical environment of the carbon atom induced by the R group of $ROCO_2Li$.

A similar study was performed on a UF_4–PVDF (3% w/w) electrode but reduced only to 0.8 V and then oxidized to 2 V.

In this case, EEL analysis indicates only the presence of Li_2CO_3 with a spectrum identical to that of Fig. 5(a). Then, the voltage plateau at 0.9 V is attributed to the formation of Li_2CO_3, the reduction of EC into alkylcarbonates occurring in a second step at potentials below 0.8 V. Similar experiments carried out with P100 fibres led to the same conclusions.

In addition to the reduction products of EC, an other phase was detected which appears as remote cylindrical particles, see the TEM micrograph presented in Fig. 7. The ED pattern of these particles shown in Fig. 8 is characteristic for f.c.c. LiCl. The presence of LiCl crystallites was previously reported during their reduction in PC–$LiClO_4$ electrolyte at the lithium and aluminium–lithium surface [22]. $LiClO_4$ is thermodynamically unstable in the presence of carbon or lithium electrode and may be reduced to LiCl.

3.3. FT-IR spectroscopy study

Previous works based on FT-IR already investigated the chemical nature of the reduction products of solvent mixtures containing EC and formed at the surface of electrodes of lithium or carbon [14,16,23].

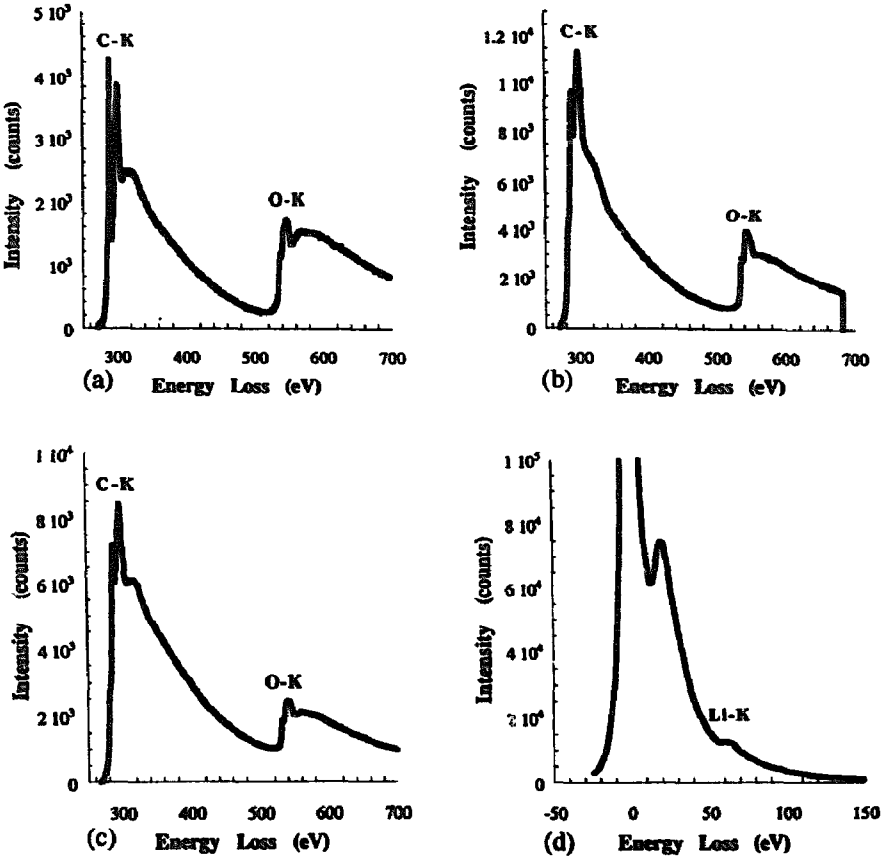

Fig. 5. EEL spectra of products observed when the composite electrode UF_4–PVDF (3% w/w) is reduced to 0.01 V and then oxidized up to 2 V in EC–$LiClO_4$ (1.5 M EC): (a)–(c) are related to different *O/C* atomic ratios, and (d) corresponds to lithium K-edge.

In order to confirm our data obtained by TEM analysis, an FT-IR study has been conducted.

Fig. 9(a) shows an FT-IR spectrum obtained by diffuse reflexion on a P100 fibres–PVDF (3% w/w) electrode after a complete first galvanostatic charge/discharge cycle between 0.01 and 2 V. The electrode material is mixed with 3 wt.% KCl. The peaks present at 1520 and 1440 (υCO_3^{2-}) are characteristic for Li_2CO_3 [23,24] while the peaks at 2958 to 2853 (υCH), 1668 cm^{-1} ($\upsilon_{as}C{=}O$) and 1330 cm^{-1} ($\upsilon_s C{=}O$) are attributed to lithium alkylcarbonates ($ROCO_2Li$) [24,25]. In the same way, the peaks corresponding to the deformation of the C–O bonds are masked by the intense bands of $LiClO_4$ around 1100 cm^{-1}.

The peak at 1778 cm^{-1} is characteristic for the solvent EC which remains adsorbed on the surface of the electrode. The peak at 2000–2100 cm^{-1} is not yet clearly identified. It could be related to the C–F vibration, present for PVDF or for its possible reduction products. We found that lithium alkylcarbonates are unstable upon heating and may decompose in the presence of H_2O giving R–OH compounds and Li_2CO_3 [16]. It is possible that the detected Li_2CO_3 is also due to the secondary reaction of $ROCO_2Li$ with trace amounts of water. After exposing the electrode in air for several hours, we found that the transformation of $ROCO_2Li$ into Li_2CO_3 is slow and therefore, it can be reasonably concluded that this detected Li_2CO_3 is mainly provided during the EC reduction process.

In the case of a P100 fibres–PVDF electrode (3% w/w) reduced to only 0.8 V and then oxidized to 2 V, the FT-IR spectrum presented in Fig. 9(b) exhibits only the peaks corresponding to Li_2CO_3 (1510, 1440 and 867 cm^{-1}) and to $LiClO_4$ (1112, 1088 and 625 cm^{-1}).

Peaks corresponding to lithium alkylcarbonates are never observed.

A similar behaviour is observed when using UF_4 as the electrode. However, because of the smaller specific area of UF_4 comparing with that of milled P100, the relative quantity of passivating layer at the UF_4 surface is smaller than at the P100 surface. Consequently, interpretation of the IR data is facilitated with the P100 based system.

Results of the FT-IR study confirm those given by TEM indicating that reduction products of the electrolytes are Li_2CO_3 and lithium alkylcarbonates. EELS study gives two values for the atomic *O/C* ratio (1.5 and 1) for these alkylcarbonates.

According to these data, we can propose the following reduction mechanism for EC. The first reduction step of the EC molecule occurs at about 0.8 V (middle value in the potential plateau) and corresponds to the formation of

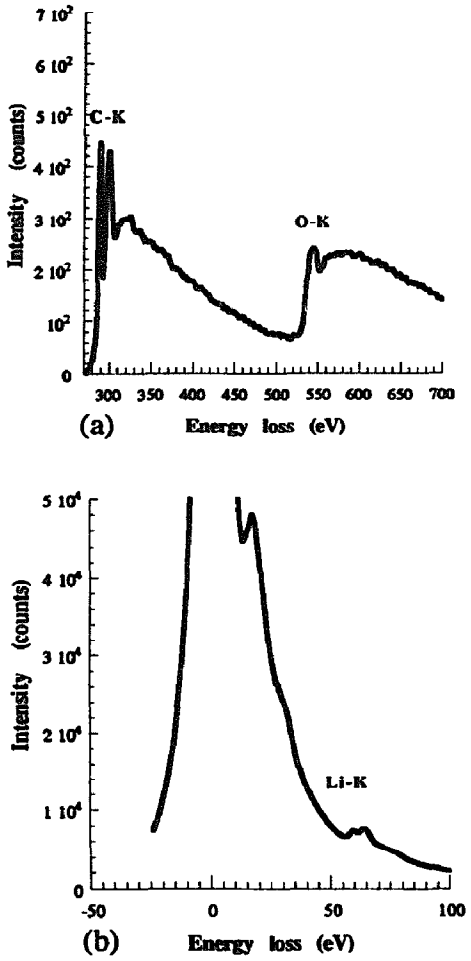

Fig. 6. EEL spectrum of Li_2CO_3 used as standard.

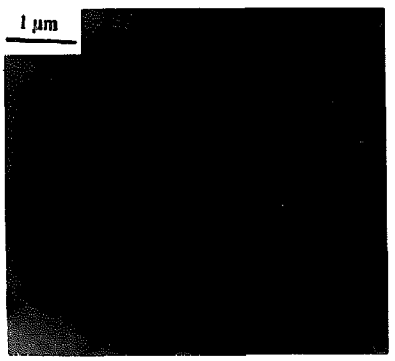

Fig. 7. TEM micrograph of lithium chloride.

Li_2CO_3 (atomic ratio $O/C=3$). The second step, below 0.8 V, corresponds to the formation of an EC anion radical which is then reorganized into different lithium alkylcarbonates ($O/C=1.5$ and 1), as presented in the following scheme:

(i) first step

$$EC+2e^-+2Li^+ \rightarrow Li_2CO_3+CH_2=CH_2\ (gas)\quad O/C=3 \qquad (2)$$

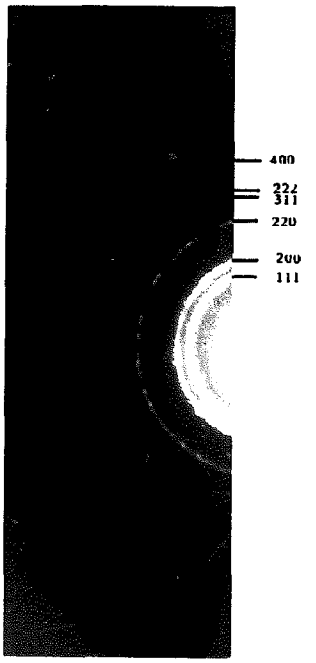

Fig. 8. ED pattern of LiCl particles shown in Fig. 7.

(ii) second step

$$EC+e^-+Li^+ \rightarrow (EC^{-\cdot}, Li^+) \qquad (3)$$

$$2(EC^{-\cdot}, Li^+) \rightarrow (-CH_2-O-CO_2Li)_2 + CH_2=CH_2\ (gas)\quad O/C=1.5 \qquad (4)$$

$$2(EC^{-\cdot}, Li^+) \rightarrow (-CH_2-CH_2-OCO_2Li)_2\quad O/C=1 \qquad (5)$$

These results present similarities with those involving the reduction of PC which seems to occur in several steps leading to the formation of Li_2CO_3 and various lithium alkylcarbonates [16,26].

4. Conclusions

Electrochemical cycling on P100 carbon fibres and UF_4 natural graphite in EC–$LiClO_4$ electrolyte confirms that the shape of the curves is strongly dependent on the nature of carbon used. Reversible capacity of P100 fibres is limited to about 70% of the theoretical value of LiC_6 whereas the use of UF_4 graphite allows to reach almost this LiC_6 value.

During the first discharge, an electrolyte reduction occurs with formation of a thin layer at the carbon surface. Both for UF_4 and P100 fibres electrodes, EEL and FT-IR spectroscopies have shown that this layer is constituted of Li_2CO_3 and different lithium alkylcarbonates ($ROCO_2Li$). This reduction seems to occur in two steps: the first step leads to the formation of Li_2CO_3 at potential above 0.8 V, followed at

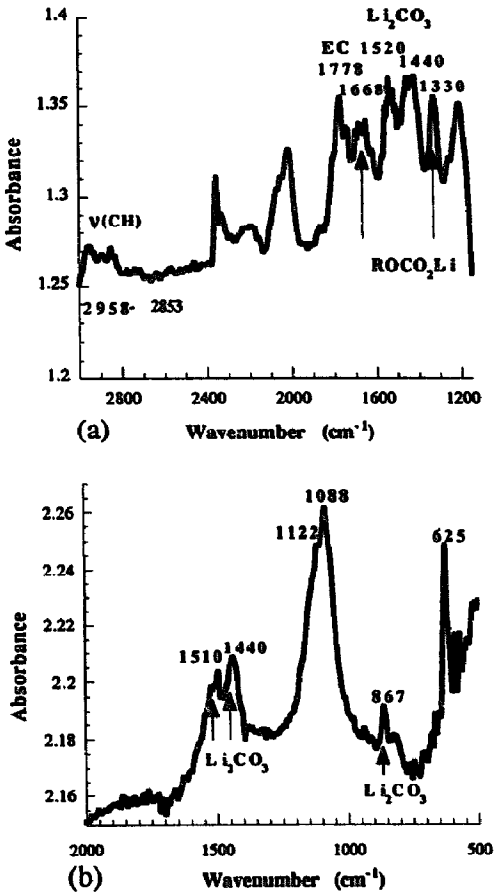

Fig. 9. FT-IR spectra of the composite electrode P100–PVDF (3% w/w) (a) after a charge/discharge cycle in EC–$LiClO_4$ (1.5 M EC) in the diffuse reflection mode (b) after a reduction to 0.8 V followed by an oxidation up to 2 V in the transmission mode.

lower potential by a second step with the formation of lithium alkylcarbonates formulated:

$(-CH_2-O-CO_2Li)_2$

and

$(-CH_2-CH_2-OCO_2Li)_2$

Remote particles of LiCl are also identified and are attributed to $LiClO_4$ reduction. Although, the surface chemistry of the Li–carbon electrode in EC based electrolyte confirms previous studies in which EC is used as the co-solvent, our studies have the particularity to use EC as a single solvent and therefore, allow a better understanding of the EC–$LiClO_4$ reduction mechanisms.

References

[1] S. Megahed and W. Ebner, *J. Power Sources, 54* (1995) 155.
[2] M. Broussely, F. Perton, P. Biensan, J.M. Bodet, J. Labat, A. Lecerf, C. Delmas, A. Rougier and J.P. Pérès, *J. Power Sources, 54* (1995) 109.
[3] R. Fong, U. Von Sacken and J.R. Dahn, *J. Electrochem. Soc., 137* (1990) 2009.
[4] Z. Ichiro Takehara and K. Kanamura, *Electrochim. Acta, 38* (1993) 1169.
[5] M. Endo, J. Ichi Nakamura, A. Emori, Y. Sasabe, K. Takeuchi and M. Inagaki, *Mol. Cryst. Liq. Cryst., 245* (1994) 171.
[6] J.R. Dahn, A.K. Sleigh, H. Shi, J.N. Reimers, Q. Zhong and B.M. Way, *Electrochim. Acta, 38* (1993) 1179.
[7] Z.X. Shu, R.S. Mc Millan, J.J. Murray and I.J. Davidson, *J. Electrochem. Soc., 142* (1995) L161.
[8] A.N. Dey and B.P. Sullivan, *J. Electrochem. Soc., 117* (1970) 222.
[9] M. Arakawa and J. Ichi Yamaki, *J. Electroanal. Chem., 219* (1987) 273.
[10] D. Aurbach and Y. Ein-Eli, *J. Electrochem. Soc., 142* (1995) .746.
[11] D. Billaud, F.X. Henry and P. Willmann, *J. Power Sources, 54* (1995) 383.
[12] D. Billaud, F.X. Henry and P. Willmann, *Mater. Res. Bull., 28* (1993) 477.
[13] K. Takei, K. Kumai, Y. Kobayashi, H. Miyashiro, T. Iwahori, T. Uwai and H. Ue, *J. Power Sources, 54* (1995) 171.
[14] Y. Ein-Eli, B. Markovsky, D. Aurbach, Y. Carmeli, H. Yamin and S. Luski, *Electrochim. Acta, 39* (1994) 2559.
[15] J.O. Besenhard, M. Winter, J. Yang and W. Biberach, *J. Power Sources, 54* (1995) 228–231.
[16] O. (Youngman) Chusid, Y. Ein-Ely, D. Aurbach, M. Babai and Y. Carmeli, *J. Power Sources, 43–44* (1993) 47.
[17] F. Egertonr, *Ultramicroscopy, 3* (1978) 243.
[18] F. Egertonr, *Electron Energy Loss Spectroscopy in the Electron Microscope*, Plenum, New York, 1986)
[19] Z.X. Shu, R.S. McMillan and J. Murray, *J. Electrochem. Soc., 140* (1993) 922.
[20] R. Yazami, K. Zaghib and M. Deschamps, *J. Power Sources, 52* (1994) 55.
[21] R. Yazami and M. Deschamps, *Mater. Res. Soc. Symp., 369* (1995)165.
[22] I. Epelbain, M. Froment, M. Garreau, J. Thevenin and D. Warin, *J. Electrochem. Soc., 127* (1980) 2100.
[23] S. Barusseau, B. Beden, M. Broussely and F. Perton, *J. Power Sources, 54* (1995) 296.
[24] D. Aurbach and H. Gottlieb, *Electrochim. Acta, 34* (1989) 141.
[25] D. Aurbach, Y. Gofer, M. Ben-Zion and P. Aped, *J. Electroanal. Chem., 339* (1992) 451.
[26] Y. Matsumura, S. Wang and J. Mondori, *J. Electrochem. Soc., 142* (1995) 2914.